High-throughput compositional mapping of phase transformation kinetics in low-alloy steel

Imed-Eddine Benrabah, Frédéric Bonnet, Benoît Denand, Alexis Deschamps, Guillaume Geandier, Hugo P. van Landeghem

Title: High-throughput compositional mapping of phase transformation kinetics in low-alloy steel

Authors: Imed-Eddine Benrabah[a], Frédéric Bonnet[b], Benoît Denand[c], Alexis Deschamps[a], Guillaume Geandier[c], Hugo P. Van Landeghem[a1]

Affiliations:

[a]Univ. Grenoble Alpes, CNRS, Grenoble INP, SIMAP, F-38000 Grenoble, France.

[b]ArcelorMittal Research, F-57280 Maizières-lès-Metz, France.

[c]Institut Jean Lamour, UMR CNRS-Université de Lorraine 7198, F-54000 Nancy, France.

Abstract:

Knowledge of phase transformation kinetics is a key point in designing steel grades, in particular modern high-performance grades, highly sought-after in energy and transportation applications. The design space for these grades is highly multi-dimensional given the numerous potential alloying elements. The characterization techniques that are usually relied on to assess transformation kinetics, such as metallography or dilatometry, are highly time consuming, due to their limitation to either a single transformation time or a single composition per experiment. The high-throughput approach showcased here overcomes those limitations by combining compositionally graded samples with time- and space-resolved in situ X-ray diffraction, yielding full kinetic records over a range of compositions in a single run. Its application to low-alloy steel required addressing specific challenges related to the reactivity and thermodynamics of the material. The transformation of austenite into ferrite was chosen to illustrate its benefits. Using the rich resulting database, the transformation mechanism was examined quasi-continuously

[1]E-mail: hugo.van-landeghem@grenoble-inp.fr

across sections of the composition space. Neither the paraequilibrium, nor the local equilibrium with negligible partitioning model, nor a transition from the former to the latter is applicable over the whole range of investigated conditions. Instead, the observed kinetics were explained by accounting for the solute drag exerted on the mobile interface. This work is a major contribution in accelerating the design of future low-alloy steel grades, involving the transformation of austenite into ferrite or any other transformation to which the present high-throughput methodology can be adapted.

Keywords: Steel; High-throughput characterization; Synchrotron X-ray diffraction; Combinatorial metallurgy; Phase transformations

1 Introduction

Steel is a critical material for modern society. It is by far the most produced type of structural metallic alloy, about 30 times more in weight than the second-ranking aluminum alloys [1]. It is all the more important because it holds a key role in addressing two of the most pressing challenges faced today: climate change and natural resource exhaustion. Steel is ideally suited for numerous transportation and energy applications given the abundance and the even distribution of most of its base minerals [2,3]. Its other key advantage is its unmatched versatility, as subtle tuning of its composition and its thermomechanical processing can yield a wide range of microstructures and corresponding mechanical properties [4]. In order to reach increasingly ambitious environmental targets, there is a strong demand for this range of properties to be expanded even further, notably in terms of strength and ductility [5]. In the recent past, innovative microstructure designs such as dual phase (DP) and transformation induced plasticity (TRIP) grades contributed to this endeavor [6]. Manufacturing these grades

relies on precise knowledge of phase transformation kinetics. For over 50 years, the latter have been investigated using conventional experimental methods such as metallography or dilatometry, which are extremely time-consuming as it typically takes months to characterize a few compositions. Alternatively, they can be estimated using models, but these require refining and calibrating with plenty of experimental data before they can be applied to practical cases with sufficient accuracy. Consequently, there is a strong appeal to novel methods for high-throughput measurement of phase transformation kinetics, which could dramatically speed-up the development of future high-performance grades [7–10].

The resource intensity of traditional kinetic investigations arises from the need to quantify the microstructure of the large number of individual samples required to finely comb both the transformation time and temperature, and more importantly, the composition space. Commercial low-alloy steel grades commonly include four or more alloying elements from about a dozen usual ones (B, C, N, Al, Si, Ti, V, Cr, Mn, Ni, Cu, Nb, Mo, W…), resulting in a many-dimension design space. Designing enhanced-recyclability grades involves an even more complex space as trace elements from scrap metal must be accounted for as well [11]. High-throughput approaches have been proposed as a solution to carry out rapid investigations of multidimensional composition spaces [12–15]. The crux of these methods is largely the sample fabrication routes on which they rely. In the context of structural materials, diffusion couples and multiples present the advantages of microstructures and sizes suited for the simulation of industrial processes and for a wide range of characterization techniques [16]. Of particular interest is their suitability for characterization by space- and time-resolved synchrotron X-ray diffraction, which enables the quantitative mapping of the phase fractions along the composition gradient. Combined with the

appropriate sample environment, such experiments can produce measurements of transformation kinetics over wide ranges of composition in a single experiment.

The application of this high-throughput methodology requires a number of conditions to be met by the compositionally graded specimens and the synchrotron experimental station. First, the composition gradient must extend over a distance several orders of magnitude larger than both the typical mass transport distance of the studied transformation and the size of the synchrotron beam. This ensures that the influence of the gradient on the studied transformation can be neglected. Second, the composition gradient must be strictly unidirectional. Combined with the first point, this allows a unique composition to be associated with each diffraction data point. Third, the sample must be maintained in an inert atmosphere during the experiment. This safeguards the metallic sample from oxidation and is especially important in the case of low-alloy steel, which is sensitive to decarburization as well [17]. Fourth, diffraction conditions should lead to circularly symmetric diffraction patterns exhibiting continuous, homogeneous Debye-Scherrer rings, which can be used to quantify phase fractions reliably. Finally, the detector acquisition rate and the translational velocity of the stage should be sufficient to capture all the stages of the considered transformation kinetics across all compositions within the gradient. While the former is usually well within the capabilities of modern equipment, the latter tends to be at the limit of commercially available parts, of the order of 1 $mm.s^{-1}$ for precisions of the order of 1 µm.

In the present study, all the afore-listed requirements were met with compositionally graded low-alloy steel samples in order to investigate the most ubiquitous transformation in steel processing [18–21], that of face-centered cubic austenite into body-centered cubic ferrite, and map its kinetics in the composition-temperature space. The outcome of the method is illustrated by

presenting the final results in two example systems, Fe-C-Ni and Fe-C-Ni-Mo. This type of information is critical in determining if and how prospective grades can be processed. Additionally, the harvested data was analyzed along calculation results based on the formalism associated to three different transformation mechanisms. The high density in the composition space of these datasets is leveraged to discuss the general validity of those mechanisms.

2 Material and Methods

2.1 Fabrication of diffusion couples

The samples used in this study were cast, hot-rolled and homogenized at 1200°C for 18 h and their initial compositions are provided in Table 1. The workflow for diffusion multiple fabrication consists of three steps as shown in Supplementary Fig. 1: solid-state diffusion bonding using uniaxial hot compression, high-temperature diffusion/decarburization to generate the substitutional composition gradients, re-carburization, and finally, grain size refinement. Since this study aims at exploring the effect of substitutional elements on intercritical ferrite growth in low-alloy steel, the diffusion multiples should contain gradients of composition for the substitutional elements with (ideally) a constant carbon content. Using the base alloys listed in Table 1, diffusion couples containing one substitutional element gradient were created by joining one binary Fe-C alloy and one ternary Fe-C-X alloy. Diffusion couples containing opposite gradients of composition can also be generated by coupling Fe-C-X_1 and Fe-C-X_2, where X_1 and X_2 are two different substitutional elements.

Table 1: Chemical compositions (wt. %) of the different base alloys used to fabricate the compositionally graded samples.

	C	Si	Mn	Mo	Cr	Ni	Al	Other	Fe
Fe-C	0.26	0.01	0.004	<0.002	<0.002	<0.002	0.003	<0.002	Bal.
Fe-C-0.2Mo	0.26	0.019	0.004	0.21	<0.002	<0.002	0.003	<0.002	Bal.
Fe-C-1Ni	0.26	0.02	0.004	<0.002	<0.002	1.05	0.003	<0.002	Bal.

Base alloy blocks of dimensions 15 × 15 × 7 mm^3 were prepared from one binary alloy Fe–0.26C (all compositions are given in wt. %) and two ternary alloys Fe–0.26C–X (X: 0.2Mo or 1.0Ni). Couples were made by assembling and processing two of these blocks together, as depicted in Supplementary Fig. 1. To this end, both mating surfaces were ground, polished, and finished down to 1 μm diamond paste using standard metallographic techniques. Solid-state bonding between different alloys was achieved using uniaxial hot compression, during which the samples were held together under a compressive stress of 20 MPa at 900°C for 1 h, in an Ar/2% H_2 atmosphere at 5 mbar, using a custom-made compression device. During this step, the couples were wrapped in tantalum foil to shield them from residual oxygen and minimize sticking to the grips.

The next step consisted in generating composition gradients of substitutional elements using diffusion at high temperature. The treatment must be carried out at a temperature where the alloy is single-phased and where the substitutional elements present sufficient mobility to form millimeter-sized gradients. These conditions are met in the high-temperature ferrite single-phase range. Given the initial carbon contents of the alloys of this study (0.26 wt. %), they could not be fully ferritized before liquid starts to form. To circumvent this obstacle, the diffusion treatment

was carried out in a decarburizing atmosphere, yielding carbon-free samples with millimeter-scale composition gradients. Subsequently, carbon was reintroduced in those samples as required using gaseous carburizing in a CO/CO_2 mixture.

The decarburization/diffusion treatments were carried out at temperatures between 1400°C and 1460°C depending on the composition of the base alloys, during 72 h, as can be seen in Supplementary Fig. 2. The furnace tube was continuously flushed with a 1000 sccm flow of Ar/2% H_2 and was kept at a 1.3 bar pressure. This pressure, higher than atmospheric, was used to prevent oxygen leaks in the furnace chamber and avoid oxidation. The samples were then carburized to 0.2 wt. %C at 1100°C for 72 h in a CO/2% CO_2 carburizing atmosphere, at a 1 bar pressure, and under a total gas flow of 204 sccm. The re-carburized samples were treated at 1300°C for 2 h in dry Ar to homogenize the carbon content over the whole sample. Supplementary Fig. 3 shows examples of the obtained composition profiles after the decarburization and re-carburization treatments of a diffusion couple between a binary Fe-C alloy and a ternary Fe-C-1Ni alloy and between two ternary systems Fe-C-1Ni and Fe-C-0.2Mo. The carbon content is measured along the gradients using electron probe microanalysis (EPMA) and was found to be about 0.2 wt. %. This carbon content is representative of commercial grades of advanced high strength steel (AHSS). Results show substitutional composition gradients several millimeters long in both cases. Such an extent is well suited for diffraction measurements using a typical 200 µm synchrotron X-ray beam, resulting in several dozen composition points per couple. Moreover, the composition profiles are continuous and without local fluctuations, which is necessary to accurately associate a unique chemical composition with each high-energy X-ray diffraction (HEXRD) measurement.

The obtained average grain size after the prolonged high-temperature treatments (72 h at 1400°C + 72 h at 1100°C) was 4-7 mm, which is not suitable for X-ray diffraction experiments. Plastic deformation should be used with caution to refine the microstructure by recrystallization, since an inhomogeneous through-thickness distribution of strain can cause a perturbation of the concentration gradient [17]. One way to refine the grain size without plastic deformation is to use rapid cycling heat treatments [22]. To this end, samples were first austenitized at 880°C for 1 min in a salt bath then water quenched to obtain a fully martensitic structure, as shown in Supplementary Fig. 4. Then, the samples were treated at 880℃ for 7 seconds followed by water quenching and the operation was repeated 5 times. The rapid cycling heat treatments allowed reducing the average grain size of the diffusion couples to 200 – 250 μm. To further refine the microstructure, diffusion couples were cold rolled with the rolling direction perpendicular to the composition gradient, to avoid any change in the composition gradient. Prior to the cold rolling step, samples were tempered at 660℃ during 5 h to generate a ductile microstructure. To avoid inhomogeneity of deformation, only 20 % of reduction was applied on the diffusion couples in a single pass. At the end, samples were treated at 900℃ for 1 min to recrystallize the microstructure. As a result, the new average grain size after rapid cyclic heat treatments and cold rolling was about 50-80 μm, which is well suited to the X-ray diffraction experiments and for the study of ferrite precipitation.

2.2 High-energy X-ray diffraction experiments

In situ high-energy X-ray diffraction experiments were performed at the beam-line P21.2 of the DESY PETRA III synchrotron in Hamburg, Germany, using an energy of 82 keV (λ = 0.1512 Å). The high-energy beam allows working in transmission mode. To maximize the number of grains in the illuminated volume, a beam size of 1 × 0.08 mm^2 (80 μm along the

concentration gradient, 1 mm perpendicularly) was used. The Debye-Scherrer diffraction rings were collected using a high-resolution 2D VAREX 4343CT detector with a 10 Hz acquisition rate placed 1 m away from the sample. NIST Standard Reference Material silicon 640d [23] and pyFAI software [24] were used to calibrate the measurement system. Cylindrical samples, 30 mm in length and 3 mm in diameter, were machined out of the diffusion couples. The sample environment for the *in situ* experiments consisted of a radiative furnace [25] with atmosphere control and sample rotation capabilities. The used rotation speed was 5 rotations/s. The rotary sample holder minimizes the potential effects of texture and coarse grain size on the diffraction patterns. Heating required for the thermal schedules shown in Fig. 1a was achieved by a set of lamps surrounding the sample and the temperature was regulated using a spot-welded type-S thermocouple. A high-purity (N60) argon flow was used to shield the sample and prevent decarburization and oxidation during the experiments. A schematic diagram of the experimental setup can be found in Fig. 1b, along with side and in-axis pictures in Fig. 1c and Fig. 1d, respectively.

The sample and furnace configuration minimized the temperature gradient over the scanned composition profile of the diffusion couple. This thermal gradient was evaluated *in situ* for the Fe-C/Fe-C-Ni couple. To this end, the control thermocouple was welded at the ternary Fe-C-1Ni composition end, providing a direct measurement at this point. The temperature at the binary Fe-C composition was estimated by matching the fraction calculated with the ThermoCalc software package with the TCFE9 database to that observed experimentally after 900 s. This temperature can be used as a measurement since the transformation is known to proceed until equilibrium values are reached in the binary system [26]. As a result, a gradient of about 1.5°C/mm was

found between the two extremities of the composition gradient. This value was assumed to hold for the Fe-C-Ni/Fe-C-Mo couple.

In order to gather time- and space-resolved ferrite growth kinetics during heat treatments, the compositionally graded samples were translated continuously along the composition gradient. The samples were scanned over several millimeters by continuous, vertical translation of the furnace at a 1 mm/s velocity. The exact position of the stage was tracked at all times using a pair of linear variable differential transformers (LVDTs). Diffraction patterns were continuously recorded during the entirety of each run with an acquisition time of 0.1 s. In this configuration, diffraction patterns were recorded every 5 to 10 s for each composition along the gradient.

The details of the heat treatments for *in situ* HEXRD experiments were as follows. The compositionally graded samples were heated to 910°C at 10°C/s and held at this temperature for 30 s to reach full austenitization, which was checked using the diffraction patterns recorded during this step. Samples were then rapidly cooled down at 60°C/s to an inter-critical temperature (between 730°C and 775°C) and held at this temperature for 15 min to follow the transformation of austenite into ferrite. Finally, samples were cooled to room temperature at 60°C/s. The protective atmosphere associated to a thermal schedule strictly limited to the needs of the experiment allowed reuse of the same graded sample, notably for the investigation of multiple temperatures. This limited the number of samples required for mapping transformation kinetics in a given composition range. The obtained Debye-Scherrer diffraction rings, as illustrated in Supplementary Fig. 5, were converted to classical 2θ-intensity diffractograms, as shown in Supplementary Fig. 6, by circular integration using the pyFAI software package [24]. Rietveld refinement was used to determine phase fractions using the FullProf software package [27]. The typical absolute observational error based on this procedure is estimated at about 1 %.

The evolution of ferrite fraction as a function of time across a diffusion couple between Fe-C and Fe-C-Ni treated at 730°C is shown in Supplementary Fig. 7. The observed oscillations in ferrite fraction correspond to the sample translation along the nickel gradient. In accordance with the high-throughput logic of the method, the obtained ferrite fractions must be sorted as function of composition. To this end, each fraction data point is first associated to a stage position by using the data from the LVDTs, which can be seen in Supplementary Fig. 8. Next, this positional information is converted into a compositional one using EPMA measurements, presented in Supplementary Fig. 9. This leads to Supplementary Fig. 10, where each curve corresponds to the evolution of ferrite fraction as a function of time for a specific nickel composition. Considering the beam size of 80 µm used during the HEXRD experiments, the variation of nickel composition within the beam is about 0.018Ni, about 2 % of the maximum content. The result clearly brings out the effect of nickel content on the ferrite growth kinetics. Ferrite growth rates, as well as the ferrite fractions reached at the plateau, decrease with increasing nickel content. This dependency of ferrite growth rate on nickel composition was obtained using a single experiment illustrating the importance of high-throughput methods on providing rich databases that can be used to understand phase transformation kinetics in steels.

Finally, the grain size of the parent austenite that underwent the transformation is needed for accurate interpretation of the data. It was measured at the end of the HEXRD experiments, continuously throughout the gradient by metallography, assuming that all ferrite nucleates at prior austenite grain boundaries. To this end, *post mortem* samples were cut in half length-wise and hot mounted before being ground on SiC paper and polished with diamond paste, down to a 1 µm finish. The ferrite/martensite microstructure resulting from the *in situ* experiment was revealed by etching the samples with a 4 % potassium metabisulfite aqueous solution.

2.3 Models of the transformation of austenite into ferrite

To analyze the data, the experimental growth kinetics is compared with the predictions of the different theoretical models: paraequilibrium (PE), local equilibrium with negligible partitioning (LENP), and solute drag. The input data for the models are carbon and nickel contents measured using EPMA, temperature and parent austenite grain size.

LENP and PE calculations were carried using the ThermoCalc software package with the TCFE9 and MOB2 databases. Parent austenite grains were assumed spherical with a thin (100 nm) initial ferrite nucleus at the grain boundaries.

Solute drag modeling was carried out using a revision of the three-jump model developed by Zurob et al. [28]. The name of the model stems from its discrete representation of the transformation interface using four atomic layers. A key feature of Zurob's model is the choice of two parameters: the binding energy of the substitutional element at the interface and its trans-interface diffusion coefficient. These two parameters are not known experimentally and generally used as fitting parameters.

According to Zurob's approach [28], the diffusion coefficients D_1 and D_3, corresponding to the first and last jumps, were taken as the diffusion coefficients of element X in ferrite D_α and in austenite D_γ, respectively. For the intermediate jump, the diffusion coefficient D_2 was systematically taken as the geometrical average of D_α and D_γ. As a result, the interface diffusion parameter is not considered as a fitting parameter, unlike in previous studies [29]. The only fitting parameter used in the present study is thus the interaction parameter between elements Fe and X at the interface. It is important to note that this parameter does not control the segregation behavior of element X at the interface alone. The segregation tendency is expressed with the combination of the different interaction parameters such as the Fe-X, Fe-C and X-C parameters.

The interaction parameter of carbon at the interface was adjusted to -50 kJ/mol to capture the significant segregation of carbon at the interface, observed notably by atom probe tomography [30]. The interactions between X and Fe, and between C and Fe are controlled using the thermodynamic parameters in the ThermoCalc database $L_{Fe,X:Va}$ and $L_{Fe,C:Va}$, respectively. Changing either or both of these parameters results in a modification of the substitutional solute-carbon (X-C) Wagner interaction parameter ϵ_{XC} in the boundary[31], which represents the interaction between solute X and carbon in the dilute solution model. To account for this change, the Wagner coefficient was calculated both in austenite and in the interface, then the $L_{Fe,X:C,Va}$ parameter of the interface was adjusted to reproduce the same Wagner interaction value as in austenite. As a result, only the $L_{Fe,X:Va}$ parameter is used as a fitting parameter. For quaternary systems, the Wagner interaction coefficient between X_1 and X_2 ϵ_{X1X2} was also modified to obtain the same value as in austenite. Indeed, this parameter is affected by changes in the $L_{Fe,X1:Va}$ and $L_{Fe,X2:Va,}$ thermodynamic parameters [31]. Thus after modifying them appropriately, the Wagner interaction coefficient between X_1 and X_2 was calculated in both austenite and the interface. The parameter $L_{X1,X2:Va}$ of the interface was adjusted to capture the same X_1-X_2 Wagner parameter as in austenite. It was found, using this approach, that quaternary cases can be modeled using the $L_{Fe,X:Va}$ parameters determined from the corresponding ternary sub-systems, thus requiring no fitting parameters.

Supplementary Fig. 11 compares the evolution of the measured ferrite growth kinetics using HEXRD and the predicted kinetics using the different models, PE, LENP and solute drag for the whole range of the studied compositions. Both LENP and PE predicted kinetics are faster than the measured ones and the discrepancy between the measurements and the calculations increases with nickel content. The predicted kinetics using the solute drag model are in good agreement

with the measurements. The Fe-Ni interaction parameter at the interface was the only fitting parameter and was kept constant over the whole composition range, from 0 to 1 wt.% Ni.

3 Results and Discussion

Fabrication of the samples is particularly challenging in this specific case due to the simultaneous presence of both carbon and substitutional alloying elements. As stated in section 1, it is necessary for the composition gradient to reach a minimal size. In the present case, this size is of the order of a centimeter. Substitutional elements are sluggish diffusers in steel [32], as it would take about a month to establish such a gradient in the austenitic range [33]. To keep diffusion treatment times under a week, it becomes necessary for them to be carried out in the high-temperature ferrite single-phase region, where they are sped up by a factor of approximately 10. However, at the carbon contents suitable for the present work, liquid forms before the samples can be fully ferritized. To circumvent this, samples were treated in a decarburizing atmosphere, yielding carbon-free samples with properly sized gradients. Subsequently, carbon was reintroduced in those samples as required using gaseous carburizing in a CO/CO_2 mixture. Carbon is an interstitial element and displays a diffusion coefficient up to six orders of magnitude greater than substitutional elements [34]. Thus, carburization can be performed in the austenite single-phase region until carbon content is homogeneous, without affecting the previously established gradient of substitutional elements. Performing those steps in single-phase regions, ferritic then austenitic, also presents the advantage of minimizing distortions in the diffusion front, as it promotes homogeneous diffusion, with the unavoidable exception of grain boundaries, and prevents alloying element partitioning in secondary phases. In the present case of a planar initial front, this leads to a quasi-unidirectional composition gradient across the sample. The requirement for a single-phase material during the heat treatment steps introduces a

limitation regarding the ranges of composition that can be investigated as it imposes that the two base alloys forming the couple present common temperature ranges over which they can both be fully ferritized and austenitized.

Equally important is the use of an appropriate sample environment for the *in situ* experiment. In the present case, the measurements were focused on the isothermal transformation of austenite into ferrite in the intercritical range. As depicted in the general thermal schedule in Fig. 1a, such experiments require fast temperature changes, 60°C.s^{-1} here, and accurate control of the temperature, within ± 1°C. Additionally, the homogeneous temperature zone must be at least as large as the composition gradients in the samples, so that all kinetic records across the gradient correspond to the same temperature. A specifically designed lamp furnace was used to apply the required sample environment shown in Fig. 1b. After experimenting with other heating methods, radiation heating was found to deliver the best compromise in terms of temperature homogeneity and heating/cooling rates. This furnace notably features a water-cooled, rotating sample holder enclosed in an amorphous silica tube. This tube is flushed with high-purity argon during thermal cycles to preserve the specimens from oxidation and decarburization. The rotation motor allows between a half and a full rotation during each diffraction pattern recording time. This feature greatly enhances the appearance of the Debye-Scherrer rings, which become much more continuous and more homogeneous compared to static recording. Fig. 1c and Fig. 1d show the furnace as setup in the experiment hutch of the synchrotron beamline.

The last items to address are the X-ray beam size as well as the pattern acquisition and scan rate, which will condition the spatial and compositional resolution of the profile. The requirements on these parameters must be tuned depending on the material and the transformation. The optimal beam size results from a compromise: a large beam gives more signal and illuminates more

grains whereas a small beam provides a higher spatial and thus compositional resolution. In the case of a unidirectional gradient, a rectangular beam was used to maximize the beam size perpendicularly to the gradient direction and minimize it parallelly. The detector acquisition rate should be as high as possible as long as diffraction patterns present high enough signal to noise ratios for accurate phase quantification. Finally, the velocity of the stage scanning the sample in front of the beam should ideally be sufficient to shift the sample by one beam size during one pattern acquisition for efficient and dense data collection. Given the acquisition rates of modern detectors, achieving such a velocity generally constitutes the most challenging hurdle, as the displacement of the stage must remain precise, within a few microns, in addition to being fast, the order of a few millimeters per second.

After circular integration of the diffraction patterns followed by phase quantification using Rietveld refinement, the typical result of the experiment is the volume fraction of the phase of interest as a function of time. This data can then be sorted based on the position of the specimen at the time of recording. In a compositionally graded specimen, each position can be further tied to a specific composition, measured using a space-resolved technique such as electron probe micro-analysis. This last step leads to full kinetic records of the transformation, quasi continuously over an entire range of composition. A typical dataset obtained after one *in situ* run is represented in Fig. 2, showing the case of a ternary graded sample transformed at 730°C.

A 4-day synchrotron time slot on beamline P21.2 at DESY was sufficient to acquire over 1500 kinetic records for independent compositions and temperatures, resulting in an amount of kinetic data that compares with the entirety of the pre-existing literature, covering the isolated effects of silicon, chromium, manganese, nickel and molybdenum, as well as several of their combinations. Additionally, measurements from the literature are usually sparse, either over time or over the

composition range [35–44]. Here, the kinetic records are dense along both dimensions. This is advantageous when they are directly used as references to estimate the transformation kinetics of a particular alloy with a much-reduced need for interpolation. It is also helpful to pinpoint transitions in the transformation mechanism more easily and with greater precision than with traditional methods. More importantly, such a database is very well suited for comparison with results from numerical models of the transformation.

In the case of the non-partitioning growth of ferrite into austenite, the two most common models are the para-equilibrium (PE) model [45] and the local equilibrium with negligible partitioning (LENP) model [46]. These models correspond to simple, extreme hypotheses regarding the transformation mechanism. Both models have been used extensively in attempts at modeling the transformation kinetics and determining which set of hypotheses is the most representative [40]. In some cases, it was concluded to a better agreement with the PE model [47], while others reported a better agreement with the LENP model [37,41,42]. There are also numerous cases in which the transformation kinetics is intermediate [34,42,43]. This led to the proposition that conditions at the interface, and thus its velocity could evolve from PE to LENP during the transformation [40]. However, there exist results where the kinetics were found to fall below the predictions of both models [42,44]. This discrepancy in reported results shows that a clear understanding of the transformation has not been achieved yet.

The results presented here can also be used to explore this question. However, instead of a few discrete points in the (time, composition) space, it is possible to compare modeling results to experimental data with both a high time resolution, of the order of a few seconds, and a high composition resolution, of the order of 0.01 wt.%.

In all examined systems and conditions, observed transformation kinetics do not match PE calculations. This is illustrated in Fig. 3a where it can be seen that, in the Fe-Ni-C system, the model predicts higher transformation rates than those that were recorded and does so even during the first seconds of the transformation by a factor of about 7. Moreover, the final ferrite fractions that it returned exceeded experimental records starting from very low substitutional solute contents, by more than 1 % at 0.1 wt.% Ni. The gap widens as this content increases as shown in Fig. 3b. The results of the model in higher-order systems compared similarly to experimental measurements. The results obtained for the Fe-Ni-Mo-C system exemplify this behavior over the entire investigated portion of the (time, composition) space, as can be noted by comparing Fig. 4a to Fig. 4b. If the transformation starts transiently under PE conditions [40], these were short-lived in the investigated cases, the order of a second or less. This supports the assumption that if interfacial concentrations match PE calculations at nucleation [40], they rapidly change during growth. LENP did not capture the kinetics of the transformation either, overestimating the transformation rates as evident from both Fig. 3a and Fig. 4c. It did predict final ferrite fractions in good agreement with the experiments at low substitutional solute contents, as seen in Fig. 3b where its predictions remain within ± 1 % from the experimental data up to 0.6 wt.% Ni. However, LENP deviates from experimental data at higher contents, by more than 2 % at 1 wt.% Ni, indicating that an alternative mechanism operates.

Other more complex models of the transformation have been proposed [28,48–50]. These models generally display a better suitability for a universal description of the transformations. The solute-drag model proposed by Zurob et al. is one such recent example [28] in which the energy dissipation due to the interaction between substitutional solutes and the moving interface accounts for the transformation kinetics. It was able to accurately describe the transformation

kinetics in many systems during decarburization. It should be noted that the better performance of this more elaborate model comes at the cost of additional, a priori unknown parameters related to the properties of the transformation interface. As they cannot be directly measured, these parameters are assessed by fitting experimental kinetic data. With sparse experimental datasets, these added parameters always lead to at least one satisfactory fit. Using large datasets such as the ones collected here permits to constrain those parameters and reduce their associated variance.

Solute-drag-based calculations were able to describe the transformation kinetics better than both PE and LENP for all solute contents using a single set of interface-related parameters. In particular, the thermodynamics used to translate the interaction between nickel (resp. molybdenum) and the interface for the calculations in the ternary Fe-Ni-C (resp. Fe-Mo-C) were kept for the calculations in the quaternary Fe-Ni-Mo-C shown in Fig. 4d. Solute drag calculations returned values closest to the experimental data over all the composition ranges, both in terms of final ferrite fraction and kinetics.

4 Conclusions

A high-throughput methodology for mapping phase transformation kinetics in the composition space was successfully applied to study the transformation of austenite into ferrite in low-alloy steel. The technique consists in in situ time- and space-resolved synchrotron X-ray diffraction experiments conducted on compositionally graded specimens. The dataset resulting from a single run is highly resolved along both composition and time dimensions. The resulting database, unprecedented in size, was compared to calculations using PE, LENP and solute drag models in example systems Fe-Ni-C and Fe-Ni-Mo-C. The main findings can be summarized as follows:

- The PE model overestimates the amount of ferrite formed at the end of the transformation, even at low solute contents. Addition of 0.1 wt.% Ni leads to an overestimation by more than 1 %. This discrepancy strengthens with increasing solute content.
- Experimental transformation rates were always lower than PE predictions even after short transformation times of the order of a second.
- LENP calculations returned ferrite fractions at the end of the transformation in good agreement with experimental observations when solute content is low. Ni contents in excess of 0.6 wt.% result in overestimation by more than 1 %.
- Solute drag simulations led to a good agreement with the experimental data over all investigated composition ranges in both Fe-Ni-C and Fe-Ni-Mo-C, never deviating by more than 1 %.

The experimental results supporting these conclusions were made possible by the high-throughput methodology developed in this work. It was shown here to provide a rapid and thorough assessment of the effect of composition on the austenite to ferrite transformation kinetics. This information is critical to manufacturing modern low-alloy steel grades and designing future ones. It should also be noted that the bases of the methodology are general and thus, it can be adapted to other phase transformation cases, in steel but also in other metallic alloys.

Data availability: The raw/processed data required to reproduce these findings cannot be shared at this time as the data also forms part of an ongoing study.

References:

[1] U.S. Geological Survey, Mineral Commodity Summaries 2020, U.S. Geological Survey, 2020. https://pubs.usgs.gov/periodicals/mcs2020/mcs2020.pdf (accessed August 24, 2020).

[2] U.S. Department of Energy, Quadrennial Technology Review 2015, U.S. Department of Energy, 2015. https://www.energy.gov/sites/prod/files/2017/03/f34/quadrennial-technology-review-2015_1.pdf (accessed August 26, 2020).

[3] A. Deschamps, G. Martin, R. Dendievel, H.P. Van Landeghem, Lighter structures for transports: The role of innovation in metallurgy, Comptes Rendus Phys. 18 (2017) 445–452. https://doi.org/10.1016/j.crhy.2017.09.006.

[4] S. Keeler, M. Kimchi, M. Peter J., Advanced High-Strength Steels Application Guidelines v6.0, WorldAutoSteel, 2017.

[5] K. Lu, The Future of Metals, Science. 328 (2010) 319–320. https://doi.org/10.1126/science.1185866.

[6] C. Lesch, N. Kwiaton, F.B. Klose, Advanced High Strength Steels (AHSS) for Automotive Applications − Tailored Properties by Smart Microstructural Adjustments, Steel Res. Int. 88 (2017) 1700210. https://doi.org/10.1002/srin.201700210.

[7] M.L. Green, I. Takeuchi, J.R. Hattrick-Simpers, Applications of high throughput (combinatorial) methodologies to electronic, magnetic, optical, and energy-related materials, J. Appl. Phys. 113 (2013) 231101. https://doi.org/10.1063/1.4803530.

[8] J.-C. Zhao, High-Throughput and Systematic Study of Phase Transformations and Metastability Using Dual-Anneal Diffusion Multiples, Metall. Mater. Trans. A. 51 (2020) 5006–5022. https://doi.org/10.1007/s11661-020-05915-w.

[9] F. De Geuser, M.J. Styles, C.R. Hutchinson, A. Deschamps, High-throughput in-situ characterization and modeling of precipitation kinetics in compositionally graded alloys, Acta Mater. 101 (2015) 1–9. https://doi.org/10.1016/j.actamat.2015.08.061.

[10] Y. Liu, Z. Hu, Z. Suo, L. Hu, L. Feng, X. Gong, Y. Liu, J. Zhang, High-throughput experiments facilitate materials innovation: A review, Sci. China Technol. Sci. 62 (2019) 521–545. https://doi.org/10.1007/s11431-018-9369-9.

[11] D. Raabe, C.C. Tasan, E.A. Olivetti, Strategies for improving the sustainability of structural metals, Nature. 575 (2019) 64–74. https://doi.org/10.1038/s41586-019-1702-5.

[12] J.-C. Zhao, Combinatorial approaches as effective tools in the study of phase diagrams and composition–structure–property relationships, Prog. Mater. Sci. 51 (2006) 557–631. https://doi.org/10.1016/j.pmatsci.2005.10.001.

[13] D. Raabe, H. Springer, I. Gutierrez-Urrutia, F. Roters, M. Bausch, J.-B. Seol, M. Koyama, P.-P. Choi, K. Tsuzaki, Alloy Design, Combinatorial Synthesis, and Microstructure–Property Relations for Low-Density Fe-Mn-Al-C Austenitic Steels, JOM. 66 (2014) 1845–1856. https://doi.org/10.1007/s11837-014-1032-x.

[14] J. García-Cañadas, N.J.E. Adkins, S. McCain, B. Hauptstein, A. Brew, D.J. Jarvis, G. Min, Accelerated Discovery of Thermoelectric Materials: Combinatorial Facility and High-Throughput Measurement of Thermoelectric Power Factor, ACS Comb. Sci. 18 (2016) 314–319. https://doi.org/10.1021/acscombsci.5b00178.

[15] F. Ren, L. Ward, T. Williams, K.J. Laws, C. Wolverton, J. Hattrick-Simpers, A. Mehta, Accelerated discovery of metallic glasses through iteration of machine learning and high-throughput experiments, Sci. Adv. 4 (2018) eaaq1566. https://doi.org/10.1126/sciadv.aaq1566.

[16] J.-C. Zhao, A Combinatorial Approach for Structural Materials, Adv. Eng. Mater. 3 (2001) 143–147. https://doi.org/10.1002/1527-2648(200103)3:3<143::AID-ADEM143>3.0.CO;2-F.
[17] I.-E. Benrabah, H.P. Van Landeghem, F. Bonnet, F. Robaut, A. Deschamps, Use of Space-Resolved in-Situ High Energy X-ray Diffraction for the Characterization of the Compositional Dependence of the Austenite-to-Ferrite Transformation Kinetics in Steels, Quantum Beam Sci. 4 (2019) 1–17. https://doi.org/10.3390/qubs4010001.
[18] M. Gouné, F. Danoix, J. Ågren, Y. Bréchet, C.R. Hutchinson, M. Militzer, G. Purdy, S. van der Zwaag, H. Zurob, Overview of the current issues in austenite to ferrite transformation and the role of migrating interfaces therein for low alloyed steels, Mater. Sci. Eng. R Rep. 92 (2015) 1–38. http://dx.doi.org/10.1016/j.mser.2015.03.001.
[19] Fundamentals of the Heat Treating of Steel, in: Pract. Heat Treat. Second Ed., ASM International, 2006: pp. 9–25. https://www.asminternational.org/documents/10192/1849770/ACF180B.pdf (accessed January 14, 2021).
[20] M. Militzer, Phase field modeling of microstructure evolution in steels, Curr. Opin. Solid State Mater. Sci. (2011) 10.
[21] H.I. Aaronson, W.T. Reynolds Jr., G.R. Purdy, Coupled-solute drag effects on ferrite formation in Fe-C-X systems, Metall. Mater. Trans. A. 35 (2004) 1187–1210. https://doi.org/10.1007/s11661-004-0294-2.
[22] R.A. Grange, The rapid heat treatment of steel, Metall. Trans. 2 (1971) 65–78.
[23] D.R. Black, D. Windover, A. Henins, D. Gil, J. Filliben, J.P. Cline, Certification of NIST Standard Reference Material 640d, Powder Diffr. 25 (2010) 187–190. https://doi.org/10.1154/1.3409482.
[24] G. Ashiotis, A. Deschildre, Z. Nawaz, J.P. Wright, D. Karkoulis, F.E. Picca, J. Kieffer, The fast azimuthal integration Python library: pyFAI, J. Appl. Crystallogr. 48 (2015) 510–519. https://doi.org/10.1107/S1600576715004306.
[25] B. Denand, M. Dehmas, E. Gautier, C. Bonnet, G. Geandier, J.-P. Sarteaux, Four d'analyse portable pour ligne de rayonnement, WO2019081266A1, 2019. https://patents.google.com/patent/WO2019081266A1/fr (accessed October 16, 2020).
[26] C. Zener, Kinetics of the decomposition of austenite, Trans. AIME. 167 (1946) 550–595.
[27] J. Rodríguez-Carvajal, Recent advances in magnetic structure determination by neutron powder diffraction, Phys. B Condens. Matter. 192 (1993) 55–69. https://doi.org/10.1016/0921-4526(93)90108-I.
[28] H.S. Zurob, D. Panahi, C.R. Hutchinson, Y. Brechet, G.R. Purdy, Self-Consistent Model for Planar Ferrite Growth in Fe-C-X Alloys, Metall. Mater. Trans. A. 44 (2013) 3456–3471. https://doi.org/10.1007/s11661-012-1479-8.
[29] C. Qiu, H.S. Zurob, D. Panahi, Y.J.M. Brechet, G.R. Purdy, C.R. Hutchinson, Quantifying the Solute Drag Effect on Ferrite Growth in Fe-C-X Alloys Using Controlled Decarburization Experiments, Metall. Mater. Trans. A. 44 (2013) 3472–3483. https://doi.org/10.1007/s11661-012-1547-0.
[30] H.P. Van Landeghem, B. Langelier, B. Gault, D. Panahi, A. Korinek, G.R. Purdy, H.S. Zurob, Investigation of solute/interphase interaction during ferrite growth, Acta Mater. 124 (2017) 536–543. https://doi.org/10.1016/j.actamat.2016.11.035.

[31] S.H. Lee, K.S. Lee, K.J. Lee, Evaluation of Wagner Interaction Parameter in Fe-Mn-Si-Nb-Ti-V-C System, Mater. Sci. Forum. 475–479 (2005) 3327–3330. https://doi.org/10.4028/www.scientific.net/MSF.475-479.3327.
[32] H.K.D.H. Bhadeshia, Diffusional formation of ferrite in iron and its alloys, Prog. Mater. Sci. 29 (1985) 321–386. https://doi.org/10.1016/0079-6425(85)90004-0.
[33] A.D. LeClaire, G. Neumann, 3.2.8 Iron group metals, in: H. Mehrer (Ed.), Diffus. Solid Met. Alloys, Springer-Verlag, Berlin/Heidelberg, 1990: pp. 124–130. http://link.springer.com/content/pdf/10.1007/10390457_36.pdf (accessed July 10, 2013).
[34] H.S. Zurob, C.R. Hutchinson, A. Béché, G.R. Purdy, Y.J.M. Bréchet, A transition from local equilibrium to paraequilibrium kinetics for ferrite growth in Fe–C–Mn: A possible role of interfacial segregation, Acta Mater. 56 (2008) 2203–2211. https://doi.org/10.1016/j.actamat.2008.01.016.
[35] G.J. Shiflet, H.I. Aaronson, Growth and overall transformation kinetics above the bay temperature in Fe-C-Mo alloys, Metall. Trans. A. 21 (1990) 1413–1432. https://doi.org/10.1007/BF02672560.
[36] S.K. Liu, L. Yang, D.G. Zhu, J. Zhang, The influence of the alloying elements upon the transformation kinetics and morphologies of ferrite plates in alloy steels, Metall. Mater. Trans. A. 25 (1994) 1991–2000. https://doi.org/10.1007/BF02649047.
[37] C.R. Hutchinson, H.S. Zurob, Y. Bréchet, The growth of ferrite in Fe-C-X alloys: The role of thermodynamics, diffusion, and interfacial conditions, Metall. Mater. Trans. A. 37 (2006) 1711–1720. https://doi.org/10.1007/s11661-006-0114-y.
[38] Y. Xia, G. Miyamoto, Z.-G. Yang, C. Zhang, T. Furuhara, Effects of Mo on Carbon Enrichment During Proeutectoid Ferrite Transformation in Hypoeutectoid Fe-C-Mn Alloys, Metall. Mater. Trans. A. 46 (2015) 2347–2351. https://doi.org/10.1007/s11661-015-2866-8.
[39] L. Wang, S. Parker, A. Rose, G. West, R. Thomson, Effects of Solute Nb Atoms and Nb Precipitates on Isothermal Transformation Kinetics from Austenite to Ferrite, Metall. Mater. Trans. A. 47 (2016) 3387–3396. https://doi.org/10.1007/s11661-016-3548-x.
[40] C.R. Hutchinson, A. Fuchsmann, Y. Brechet, The diffusional formation of ferrite from austenite in Fe-C-Ni alloys, Metall. Mater. Trans. A. 35 (2004) 1211–1221. https://doi.org/10.1007/s11661-004-0295-1.
[41] A. Phillion, H.S. Zurob, C.R. Hutchinson, H. Guo, D.V. Malakhov, J. Nakano, G.R. Purdy, Studies of the influence of alloying elements on the growth of ferrite from austenite under decarburization conditions: Fe-C-Ni alloys, Metall. Mater. Trans. A. 35 (2004) 1237–1242. https://doi.org/10.1007/s11661-004-0297-z.
[42] M. Enomoto, Comparison of Alloy Element Partition Behavior and Growth Kinetics of Proeutectoid Ferrite in Fe-C-X Alloys with Diffusion Growth Theory, Trans. Iron Steel Inst. Jpn. 28 (1988) 826–835. https://doi.org/10.2355/isijinternational1966.28.826.
[43] C. Capdevila, J. Cornide, K. Tanaka, K. Nakanishi, E. Urones-Garrote, Kinetic Transition during Ferrite Growth in Fe-C-Mn Medium Carbon Steel, Metall. Mater. Trans. A. 42 (2011) 3719. https://doi.org/10.1007/s11661-011-0650-y.
[44] J.R. Bradley, H.I. Aaronson, Growth kinetics of grain boundary ferrite allotriomorphs in Fe-C-X alloys, Metall. Trans. A. 12 (1981) 1729–1741. https://doi.org/10.1007/BF02643755.
[45] A. Hultgren, Isothermal transformation of austenite, Trans. Am. Soc. Met. 39 (1947) 915–1005.

[46] G.R. Purdy, D.H. Weichert, J.S. Kirkaldy, The Growth of Proeutectoid Ferrite in Ternary Iron-Carbon-Manganese Austenites, Trans. Metall. Soc. AIME. 230 (1964) 1025–1034.
[47] G. Inden, C. Hutchinson, Interfacial conditions at the moving interface during growth of ferrite from austenite in Fe-C-(X) alloys, in: E.B. Damm, M.J. Merwin (Eds.), Austenite Form. Decompositon, The Minerals, Metals & Materials Society, Chicago, IL, 2003: pp. 65–79. https://research.monash.edu/en/publications/interfacial-conditions-at-the-moving-interface-during-growth-of-f (accessed January 20, 2021).
[48] J. Sietsma, S. van der Zwaag, A concise model for mixed-mode phase transformations in the solid state, Acta Mater. 52 (2004) 4143–4152. https://doi.org/10.1016/j.actamat.2004.05.027.
[49] J. Ågren, A simplified treatment of the transition from diffusion controlled to diffusion-less growth, Acta Metall. 37 (1989) 181–189. https://doi.org/10.1016/0001-6160(89)90277-0.
[50] J. Odqvist, B. Sundman, J. Ågren, A general method for calculating deviation from local equilibrium at phase interfaces, Acta Mater. 51 (2003) 1035–1043. https://doi.org/10.1016/S1359-6454(02)00507-4.

Acknowledgments: We acknowledge DESY (Hamburg, Germany), a member of the Helmholtz Association HGF, for the provision of experimental facilities. Parts of this research were carried out at PETRA III and we would like to thank Dr. U. Lienert and Dr. Z. Hegedues for assistance in using beamline P21.2. Prof. H.S. Zurob is acknowledged for stimulating discussion and valuable input regarding solute drag modeling. Dr. Florence Robaut is acknowledged for her support with the EPMA measurements. This work was supported by the ANR (Agence Nationale de la Recherche [ANR-15-IDEX-02] and by MIAI@Grenoble Alpes [ANR-19-P3IA-0003].

Author contributions: I.-E. Benrabah: Formal analysis, Investigation, Methodology, Visualization, Writing - Review & Editing. F. Bonnet: Resources, Writing - Review & Editing. B. Denand: Investigation, Writing - Review & Editing. A. Deschamps: Conceptualization, Supervision, Writing - Review & Editing. G. Geandier: Formal analysis, Writing - Review & Editing. H.P. Van Landeghem: Conceptualization, Supervision, Writing – original draft.

Competing interests: The authors declare no competing interests.

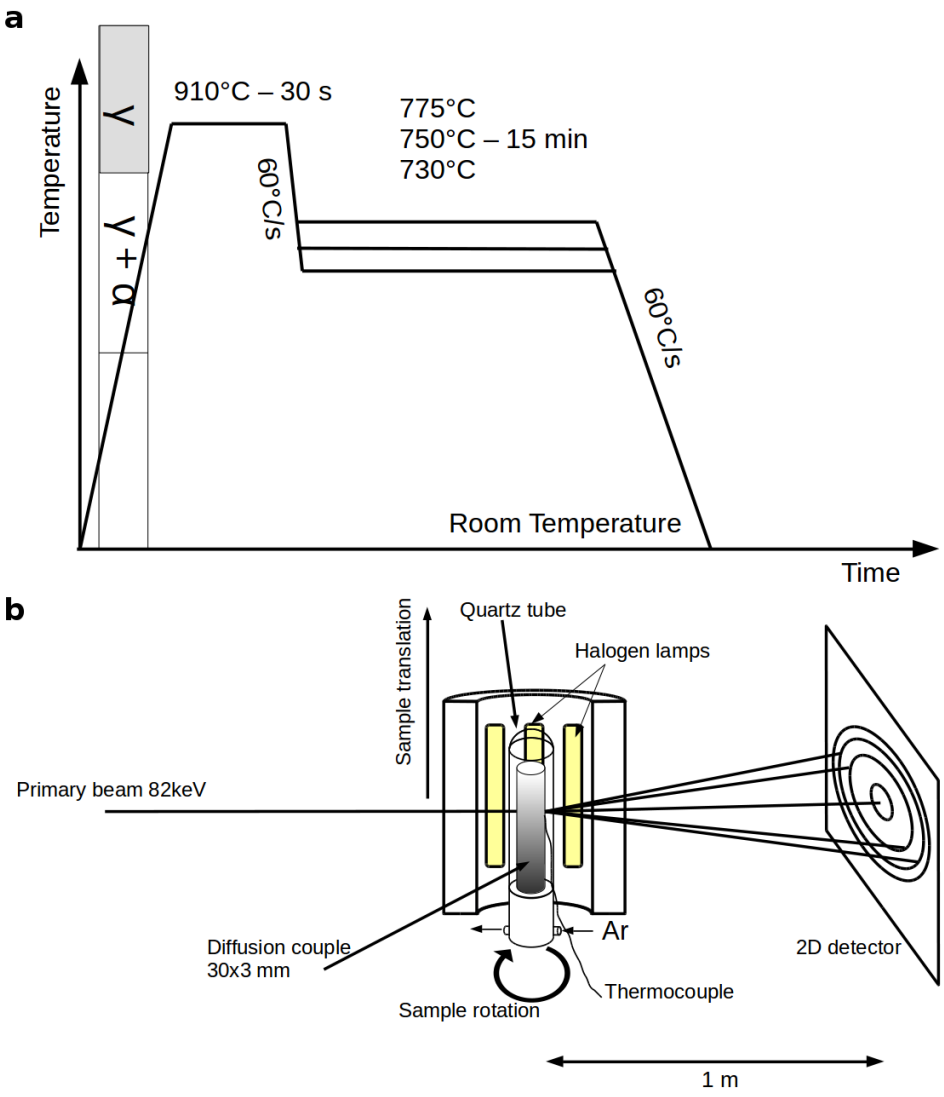
a
Temperature
γ
γ + α
910°C – 30 s
60°C/s
775°C
750°C – 15 min
730°C
60°C/s
Room Temperature
Time
b
Sample translation
Quartz tube
Halogen lamps
Primary beam 82keV
Diffusion couple
30x3 mm
Ar
Thermocouple
Sample rotation
2D detector
1 m

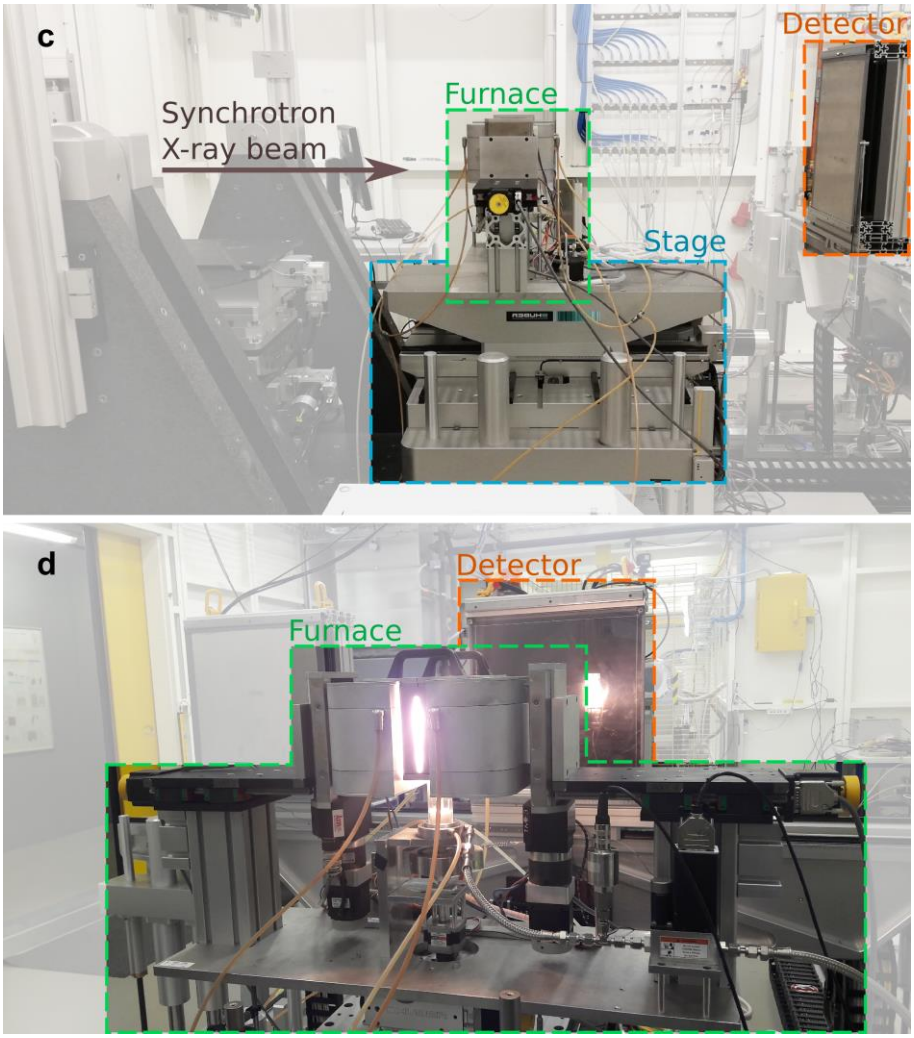

Fig. 1. Details of the *in situ* experiments. (**a**) Thermal schedules applied to the graded samples. They were designed to produce isothermal growth of ferrite from a fully austenitic microstructure. (**b**) Schematic depiction of the synchrotron sample environment on the beam line. (**c**) Picture of the experimental setup in the beamline hutch, taken perpendicular to the X-ray beam. (**d**) Picture of the furnace in operation, taken almost parallel to the X-ray beam.

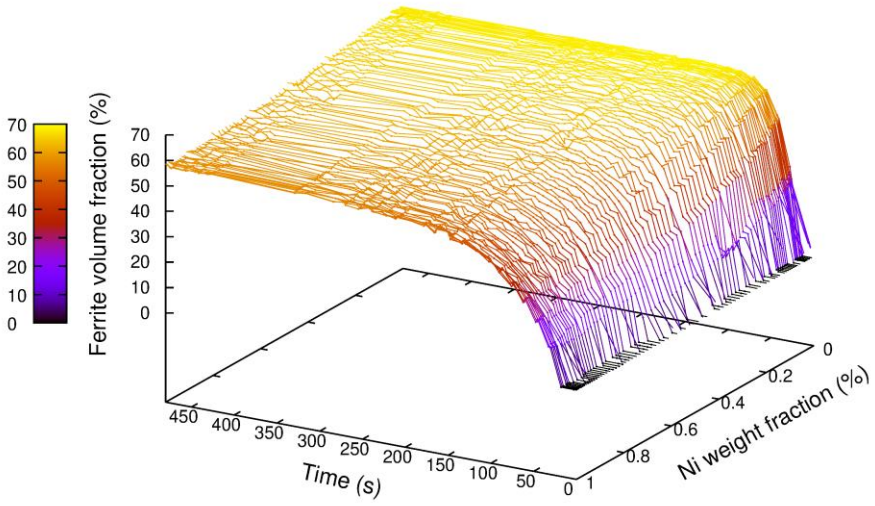

Fig. 2. Austenite-to-ferrite transformation kinetics at 730°C in a Fe-Ni-0.26C with a nickel composition gradient. The increasing nickel content decreases the tranformation rate and the final ferrite fraction.

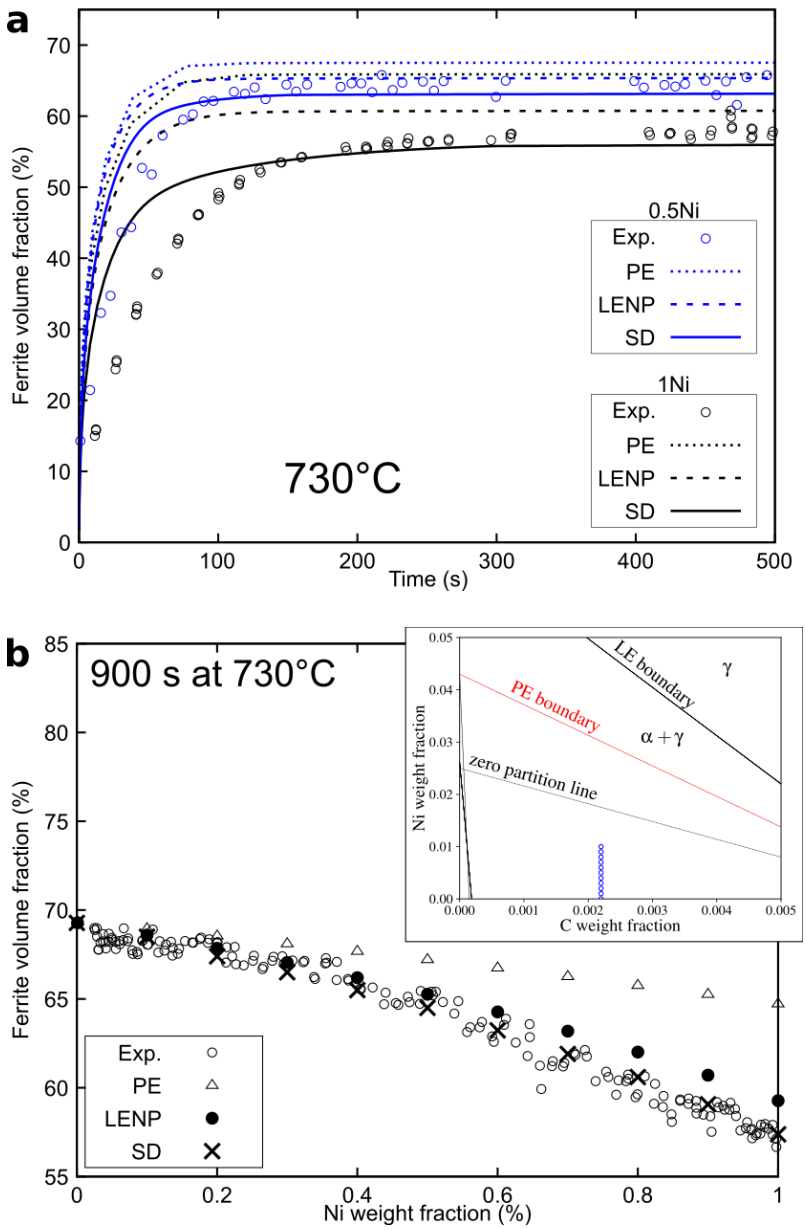

Fig. 3. Experimental volume fractions recorded during ferrite growth in an Fe-C-Ni alloy at 730°C, compared against predictions from para-equilibrium (PE), local equilibrium with negligible partitioning (LENP), and solute drag (SD) models. (**a**) Ferrite growth kinetic records of at 0.5 wt. % and 1.0 wt. % nickel contents. (**b**) Ferrite volume fractions at the end of the 900 s isothermal hold as a function of nickel content. The insert shows the position of the investigated range of compositions on the isothermal section of the ternary phase diagram.

Unlike the other models, final ferrite fractions predicted by the SD model remain within ± 1 % from the experimental values.

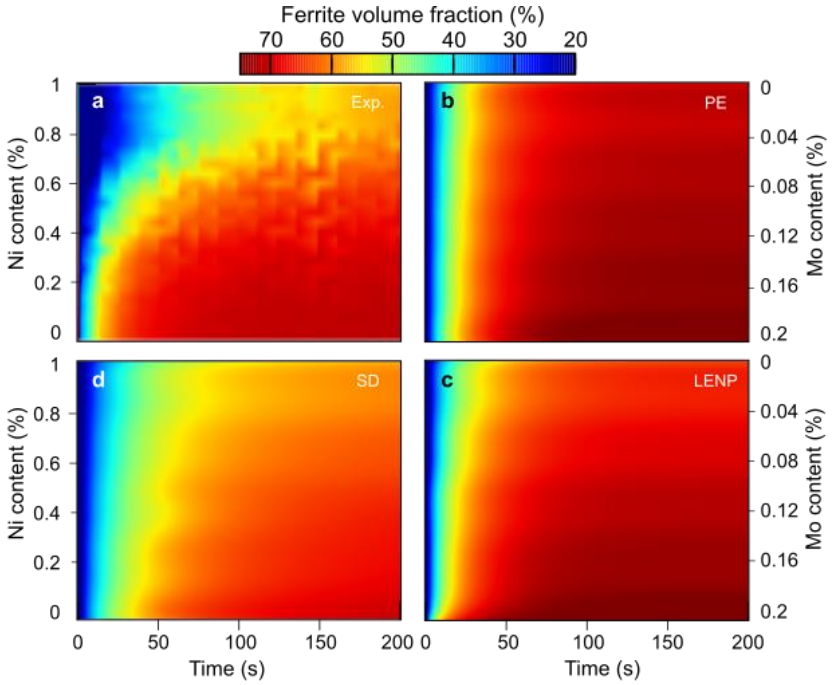

Fig. 4. Full kinetic maps of the transformation of austenite into ferrite at 730°C in the (time, composition) space in a Fe-Ni-Mo-C sample with a nickel/molybdenum gradient as given by (a) the experiment and the (b) paraequilibrium (PE), (c) local equilibrium negligible partitioning (LENP), and (d) solute drag (SD) models. SD calculations closely track experimental measurements, while the PE and LENP models overestimate both the transformation rates and the final ferrite fraction. The final fractions given by the SD model are all within ± 1 % from the experimental results, while PE and LENP results exceeds them by at least 2 % over the whole composition range. The non-monotonic evolution of the kinetics is related to local variations of carbon content, temperature and grain size.